Analytica Chimica Acta 1148 (2021) 238194

Contents lists available at ScienceDirect

Analytica Chimica Acta

journal homepage: www.elsevier.com/locate/aca

Fluorometric detection of cancer marker FEN1 based on double-flapped dumbbell DNA nanoprobe functionalized with silver nanoclusters

Bingzhi Li [a, *, 1], Peng Zhang [a, d, 1], Bin Zhou [b], Siying Xie [a], Anqi Xia [a], Tiying Suo [a], Shuang Feng [c, **], Xing Zhang [a, ***]

[a] School of Food Science and Pharmaceutical Engineering, Nanjing Normal University, Nanjing, 210023, China
[b] NHC Key Laboratory of Nuclear Medicine, Jiangsu Key Laboratory of Molecular Nuclear Medicine, Jiangsu Institute of Nuclear Medicine, Wuxi, 214063, China
[c] Department of Encephalopathy, Nanjing Hospital of Chinese Medicine Affiliated to Nanjing University of Chinese Medicine, Nanjing, 210001, China
[d] Jiangsu Conat Biological Products Co., Ltd., Shugang Road 20, Taixing, 225400, China

HIGHLIGHTS

- Nanoprobe for the recognition of FEN1 was rationally designed.
- DNA-AgNCs are first used to develop a biosensor for the detection of FEN1.
- Facile detection of cancer marker FEN1 was realized.
- FEN1 can catalyze the cleavage of nanocluster-functionalized 5′ flap.

GRAPHICAL ABSTRACT

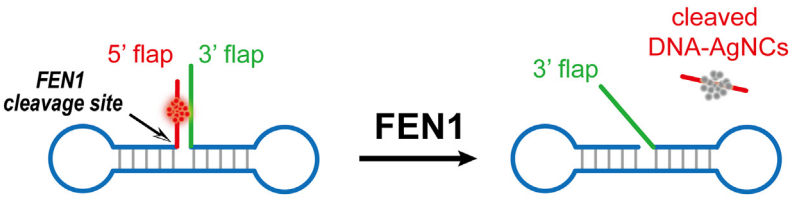

ARTICLE INFO

Article history:
Received 18 August 2020
Received in revised form
26 December 2020
Accepted 29 December 2020

Keywords:
Flap endonuclease 1
Silver nanocluster
Cancer biomarker
Functional nucleic acid
Biosensor
Aptamer

ABSTRACT

Flap endonuclease 1 (FEN1), a ubiquitous enzyme involved in DNA repair and replication, is overexpressed in highly proliferative cancer cells. FEN1 has been recognized as a promising diagnostic marker of cancers; however, very few analytical techniques have been developed for the convenient detection of FEN1. To realize the simplified quantification of FEN1, we developed a FEN1-responsive fluorescent nanoprobe based on DNA-silver nanoclusters (DNA-AgNCs). The nanoprobe was rationally designed with a double-flapped dumbbell conformation, where its 5′ flap was produced with DNA-AgNCs, and the 3′ flap was elongated by a guanine-rich enhancer sequence (GRS). Rigidified by the DNA scaffold, DNA-AgNCs and the GRS are in close proximity, resulting in high fluorescence because of the GRS-induced activation of DNA-AgNCs. Upon the addition of FEN1, the 5' flap of the nanoprobe is cleaved due to the structure-specific endonuclease activity of FEN1. This cleavage released the DNA-AgNCs from the nanoprobe, broke the proximity between DNA-AgNCs and the GRS, and caused decreased fluorescence. This nanoprobe can be applied in the sensitive detection of FEN1 with a detection limit of 40 fM, and it showed high specificity for the monitoring of FEN1 in clinical samples. As the first attempt to develop biosensors targeting FEN1 based on DNA-AgNCs, this work provided a potent platform for monitoring FEN1 and screening FEN1 inhibitors.

1. Introduction

Determining the relationship between the expression of biomolecules and pathological progress is an essential task in the era

* Corresponding author.
** Corresponding author.
*** Corresponding author.
E-mail addresses: bingzhili@njnu.edu.cn (B. Li), fengshuang_njmu@163.com (S. Feng), zhangxing@njnu.edu.cn (X. Zhang).
[1] B.L. and P.Z contributed equally to this work.

https://doi.org/10.1016/j.aca.2020.12.069
0003-2670/

of precision medicine; thus, rationally designed molecular probes are needed for detecting biomarkers [1–6]. Flap endonuclease 1 (FEN1), which is critical for almost all cell processes [7], is ubiquitously distributed in all proliferative tissues because of its involvement in long-patch base excision repair (LP-BER) and DNA replication [8,9]. DNA replication produces ~50 million Okazaki primers per cell cycle, and FEN1 is the key nuclease to remove these primers [10]. FEN1 can catalyze the removal of single-stranded DNA (ssDNA) elongated at the 5′ end of forked structures [11,12], and the FEN1-recognizable structure is referred to as the 5' flap [13]. In cancer cells, FEN1 expression increases to maintain their high proliferation ratio, and the upregulation of FEN1 levels is related to tumor aggressiveness [14,15]. Therefore, FEN1 has been recognized as a biomarker for the diagnosis and prognosis of breast, brain, prostate, and testicular cancers [16–18]. FEN1 is also a potential target in chemotherapy because the inhibition of FEN1 can suppress the rapid growth of tumors [19]. Therefore, it is important to monitor the expression levels of FEN1, which is a type of biomolecule that is crucial in clinical fields.

Currently, analytical techniques for the detection of FEN1 have been slowly developed. Conventional assays, including Western blotting, enzyme-linked immunosorbent assay (ELISA), and immunohistochemistry, have been widely adopted by investigators with a biomedical background [20,21]; however, these multistep and cumbersome assays cannot rapidly and precisely detect biomolecules in clinical applications. A few novel methods have been proposed recently to overcome the limitations of conventional methods. The Lu and Li group developed a nanobiosensor consisting of graphene oxide (GO) and a flapped DNA probe for the detection of FEN1 [22], which can be used in the imaging of FEN1 in living cells. Wei et al. designed a probe composed of gold nanoparticles, functional DNA, and organic dyes to quantify FEN1 in biological samples [23]. These two attempts have significantly simplified the analytical procedures for detecting FEN1; however, they both involve assembling multiple components and using organic dyes. The undesired influence of interferents could impede the analytical specificity, and the organic dyes could increase the cost and toxicity [24–28]. Therefore, new types of analytical devices are urgently needed to detect FEN1 with improved performance.

As a bioderived fluorescent nanomaterial, DNA-silver nanoclusters (DNA-AgNCs) have attracted substantial research attention in analytical fields [29,30]. With small size (~2 nm) and abundant surface functionalization, DNA-AgNCs are stable and have a controllable fluorescence emission [31]. DNA-AgNCs are more resistant to photobleaching than organic dyes [32–34], and their emission is related to the DNA sequences used for stabilizing the DNA-AgNCs [35]. In addition, the formation of AgNCs on the nucleation domain has no significant influence on the other parts of a DNA molecule; thus, the remaining DNA domains still can fold and hybridize [29,31,36,37]. DNA-AgNCs can serve as a stable fluorescent label with a wide range of emission wavelengths from ultraviolet to near-infrared [38]. In particular, certain kinds of DNA-AgNCs have tunable fluorescence, in which the fluorescence is related to the distance between the DNA-AgNCs and the specific DNA sequences [36]. Yeh et al. discovered that the weak fluorescence of DNA-AgNCs protected by the C34 domain can be turned on upon its proximity to a guanine-rich enhancer sequence (GRS), and this tunable emission enabled a large signal-to-noise ratio that was 500-fold higher than that of regular fluorescence resonance energy transfer (FRET) [39]. Although the underlying mechanism of this intensive fluorescence enhancement remained unclear, studies have suggested that the phenomenon is related to the transition of electronic states [34,40]. Besides, alteration of the maximum emission and the enhancement ratio can be realized by changing the sequence of DNA protecting the AgNCs [35]. DNA-AgNCs have been recognized as an ideal nanomaterial for the functionalization of DNA molecules, and have been applied in the sensing of analytes recognizable by aptamers [29,41–43]. It is worth developing aptamer-free sensors based on the intrinsic features of DNA-AgNCs.

In this work, we utilized the specific features of DNA-AgNCs and developed a DNA-AgNCs-functionalized double-flapped dumbbell nanoprobe for sensing the cancer marker FEN1. By well-controlled annealing and on-situ nucleation, DNA-AgNCs were formed at the 5′ flap of the nanoprobe, juxtaposed to the GRS located on the 3' flap. The design of this probe was based on an assumption that the formation of DNA-AgNCs on the DNA scaffold would not influence the catalytic activity of FEN1. Through experimental verification, this assumption was verified, and we found that FEN1 can cleave DNA-AgNCs from the dumbbell probe, thereby separating DNA-AgNCs from the GRS and causing fluorescence decrease. The rapid quantification of FEN1 was realized with this design, and FEN1 can be detected with picomolar sensitivity in both cell extracts and clinical samples. This is the first attempt to develop DNA-AgNCs sensors targeting FEN1 based on DNA-AgNCs, and this study broadens the application scope of DNA-AgNCs and expands the analytical techniques for FEN1 at the same time.

2. Experimental section

2.1. Materials

Oligonucleotides were synthesized and purified by Sangon Biotech (Shanghai, China), and their sequences are listed in Table S1. $AgNO_3$ (metal basis, 99.999%) and $NaBH_4$ (analytical grade) were purchased from Aladdin (Shanghai, China). All the reagents used for preparing buffers are supplied by Sangon Biotech. Recombinant human flap endonuclease 1 (FEN1), phi29 DNA polymerase, T4 DNA ligase, and nucleoprotein extraction kit were obtained from BBI (Shanghai, China). HeLa nuclear extract was supplied by Active Motif (CA, U.S.A.). Glioma samples were gathered from Nanjing Hospital of Chinese Medicines with the approval of the Ethics Review Committee of Biomedical Experiments at Nanjing Normal University (IRB-202003002). Ultrapure water used throughout this research is prepared by a Millipore's Milli-Q system (MA, U.S.A.). Diethyl pyrocarbonate (DEPC, BBI) was used to treat the water in DNA-related experiments.

2.2. Preparation of the nanoprobe

The nanoprobe was prepared according to former literature with modifications in the nucleation reaction [24,39,44]. The oligonucleotides template was dissolved to 10 μM by citrate buffer (10 mM, pH = 7.0). To obtain the double-flapped dumbbell DNA nanostructure, the solution of oligonucleotides was heated to 95 °C for 5 min, and then gradually cooled to 25 °C for at least 1 h. Afterward, freshly prepared $AgNO_3$ (1 mM) was quickly added into the above solution, followed by centrifuging at 10,000 rpm, and incubation for 15 min at room temperature. Then, 1 mM of freshly prepared $NaBH_4$ was quickly dispersed to the solution, followed by vigorous vortex and shaking for 2 min and centrifuge at 12,000 rpm for another 1 min. After aging the supernatant for 6 h at 4 °C, the solution was used without further treatment.

2.3. Gel electrophoresis

Native-PAGE (10%) gel supplied by Sangon Biotech was used in gel electrophoresis. Samples were mixed with 5 × loading buffer (20% ficoll, Sangon) and loaded in a volume of 25 μL and ran in 0.5 × TBE buffer at 120 V for 1 h. After staining with 4S Red Plus

nucleic acid stain (BBI) for 40 min, the gel image was photographed by a 3500R Gel Image System (Tanon, Shanghai, China).

2.4. Protocols for the detection of FEN1

For the detection of FEN1, 10 μL of nanoprobe (100 nM), 10 μL of the test sample, and 30 μL of reaction buffer (15 mM KCl, 30 mM Tris-HCl, 15 mM $(NH_4)_2SO_4$, 3 mM $MgSO_4$, pH 7.4) were mixed. After incubation at 37 °C for 30 min, the fluorescence was measured by an F-7100 fluorescence spectrometer (Hitachi, Japan) with excitation at $\lambda = 580$ nm. Quick and high throughput detection was conducted on an Infinite M − 200 fluorescent plate reader (Tecan, Switzerland), and the wavelength for excitation and emission were set at $\lambda = 580$ nm and $\lambda = 631$ nm, respectively. The fluorescence change (FL change) in this research was calculated by:

$$\text{FL change} = (F_0 - F_1)/F_0 \times 100\%$$

Where F_0 and F_1 represent the fluorescence before and after the addition of analytes, respectively.

The ELISA quantification kit for human FEN1 was purchased from LifeSpan Biosciences (WA, U.S.A.). The concentration of samples was quantified and unified with the Bradford protein assay (BBI) before analyses according to the manufacturer's protocols.

3. Results and discussion

3.1. The principle for this method

In this research, a DNA-AgNCs-functionalized dumbbell DNA nanoprobe was produced for the detection of FEN1. The nanoprobe was annealed to a dumbbell conformation with flapped overhangs at both the 3′ and 5′ ends. The flap at the 5′ end was a C34 domain (5′-CCCTTAATCCCC-3′) with the ability to provide a scaffold for DNA-stabilized AgNCs [39,45]. Under the treatment of Ag^+ and $NaBH_4$, *in situ* reduction and nucleation of Ag occurs at the C34 domain to form fluorescent DNA-AgNCs. The flap at the 3′ end was a GRS that can enhance the fluorescence of DNA-AgNCs *via* the transition of electronic states [24,46]. The dumbbell conformation of the nanoprobe can assist in the stabilization of the DNA-AgNCs and GRS, resulting in a high fluorescence signal derived from the approaching between DNA-AgNCs and GRS [36].

As shown in Scheme 1a, the enzymatic activity of FEN1 is to recognize the structure at the 5′ flap of the branched DNA and remove the ssDNA flap *via* conformational-specific cleavage, which plays critical roles in the removal of Okazaki fragments in cell proliferation [23]. Based on this activity, we expected that the DNA scaffold of the DNA-AgNCs located at the 5' end would be cleaved when FEN1 interacts with the nanoprobe. As illustrated in Scheme 1b, the cleavage separates DNA-AgNCs from the dumbbell DNA nanostructure, thus increasing the distance between DNA-AgNCs and the GRS. As a result, the electronic transition between DNA-AgNCs and the GRS is inhibited; the fluorescence of the nanoprobe is decreased. Under this design, the nanoprobe cleavage and the decrease in the fluorescence are proportional to the cleavage by FEN1, thereby forming a reaction system to probe the concentration of FEN1.

3.2. Verification of this method

As shown in Fig. 1a, the transmission electron microscope (TEM) image reveals that the average diameter of the obtained nanoprobe was ~2 nm, which is in accordance with results from previous reports [39]. This diameter is close to the Fermi wavelength of electrons, which imparts DNA-AgNCs with molecular-like optical properties including fluorescence [33,47,48]. The elemental composition of the nanoprobe was inspected by X-ray photoelectron spectroscopy (XPS), and Figure S1 shows that the nanoprobe contains elements, including Ag, C, N, P, and O. In particular, the P 2p peak at 133.1 eV indicated the presence of phosphate groups from DNA [49]. The peaks at 367.7 eV and 373.6 eV are Ag 3d peaks (Fig. 1b), demonstrating the occurrence of both Ag(I) and Ag (0) in the nanoprobe [50], which has been reported in the XPS study of DNA-AgNCs [51]. Fluorescence spectroscopy showed that the maximum emission of the nanoprobe is located at 631 nm under excitation at 580 nm (Fig. 1c, black curve), which is the featured fluorescent emission of GRS-activatable DNA-AgNCs [24,52]. To further confirm that the fluorescence was derived from the proximity between DNA-AgNCs and the GRS, a complementary DNA strand (s-nanoprobe) that can be stably hybridized with the nanoprobe and open the dumbbell conformation was added to the reaction. As shown in the red curve of Fig. 1c, the emission at 631 nm significantly decreased, indicating that the opening of the dumbbell structure of the nanoprobe caused a decrease in fluorescence. The opening and straightening of the nanoprobe caused the separation of DNA-AgNCs and the GRS, and the separation-derived fluorescent change is the featured property of DNA-AgNCs. These results demonstrated that the dumbbell DNA was successfully functionalized with DNA-AgNCs, forming the nanoprobe. After the introduction of FEN1, a sharp decrease in fluorescence was recorded (Fig. 1c, blue curve), which indicated that the fluorescence of the nanoprobe can be regulated by FEN1. To further demonstrate that the fluorescent decrease is the result of FEN1-induced cleavage of the DNA-AgNCs at the 5' flap, the 3-dimensional spectra of the nanoprobe before and after the addition of FEN1 were scanned. As shown in Figure S2, the excitation/emission center of the nanoprobe was at 580/631 nm with high fluorescence intensity, while the addition of FEN1 made the excitation/emission center shifted to 460/543 nm with the decreased intensity. These changes in fluorescent properties are in line with the tunable fluorescence of DNA-AgNCs that is regulated by GRS [35,46,52], which suggests that the FEN1 reduced the fluorescence of the nanoprobe by moving the DNA-AgNCs away from the GRS.

We then used gel electrophoresis to test whether the signal change was the result of FEN1-induced cleavage. The nanoprobe was treated with different concentrations of FEN1, and then the samples were analyzed by native-PAGE (Fig. 1d), a gold standard in nucleic acid research. Previous reports have demonstrated that the *in situ* synthesis of AgNCs in the DNA scaffold caused no significant changes in the migration rate of DNA [43,53], so this technique has been widely used in visualizing reactions related to DNA-AgNCs [24,31,54]. The band in Lane 1 was single and bright, indicating that the dumbbell conformation of the DNA scaffold was uniformly formed after the annealing process, and the nucleation of AgNCs on the C34 domain did not disturb the conformational uniformity. In Lanes 2−4, the addition of FEN1 weakened the band representing the nanoprobe, and two products including a fragment with a size similar to the nanoprobe were generated, and a smaller fragment exhibited high migration speed. It was assumed that the larger product was the 5′ flap-removed dumbbell DNA and that the smaller product was the cleaved DNA-AgNCs. Importantly, with increasing concentrations of FEN1, the bands corresponding to the nanoprobe gradually faded, and the bands of both the 5′ flap-removed dumbbell DNA and the cleaved DNA-AgNCs intensified accordingly. The results of native-PAGE revealed that FEN1 can cleave the nanoprobe, producing two fragments. Combining the results of fluorescent spectra and native-PAGE, it could be concluded that FEN1 decreases the fluorescence of the nanoprobe by cutting DNA-AgNCs at the 5' flap, thus verifying the mechanism of this nanoprobe in the detection of FEN1.

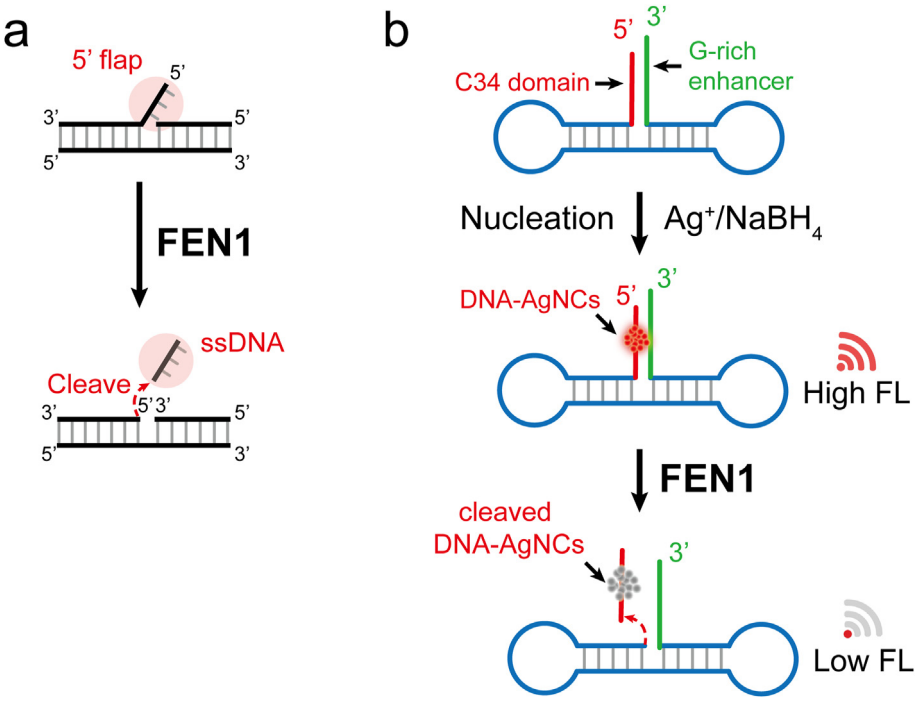

Scheme 1. (a) The illustration of the activity of FEN1. (b) Principle of the nanoprobe in the detection of FEN1. The nanoprobe was designed to be responsive to FEN1, where the DNA-AgNCs at the 5′ end would be cleaved by FEN1 to separate from the GRS.

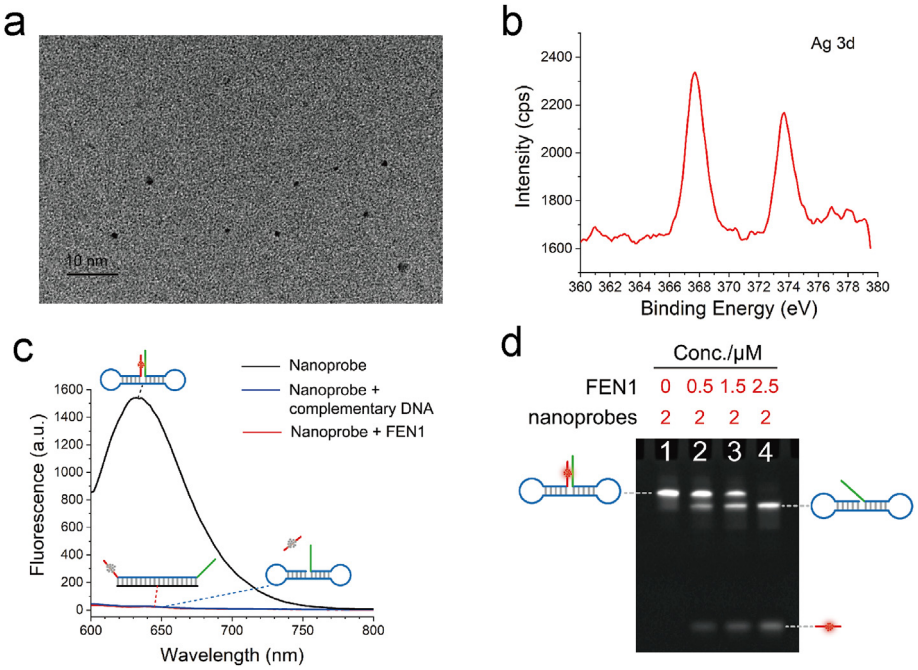

Fig. 1. Characterization of the nanoprobe and Verification of this method in the detection of FEN1. (a) TEM image of the nanoprobe. (b) The Ag 3d XPS spectrum of the nanoprobe. (c) Fluorescent spectra of the nanoprobe under different conditions (λ_{ex} = 580 nm). The concentration of nanoprobe, complementary DNA (s-nanoprobe), and FEN1 were all 50 nM. (d) Verifying the nanoprobe in the detection of FEN1 with native-PAGE. The samples were incubated at 37 °C for 1 h before gel electrophoresis.

3.3. Optimization of nanoprobe and sensing conditions

To investigate whether the formation of DNA-AgNCs on the 5′ flap affects the cleavage of FEN1 towards the DNA molecule, we designed a set of nanoprobes by adding different numbers of thymine (T) nucleotides between the C34 domain and the dumbbell substrate. The use of T nucleotides can minimize the influence on DNA-AgNCs formation because T has a weak interaction with Ag^{+} [38]. Additionally, and the conformation of the nanoprobe would not be significantly influenced by poly(T) because of the lack of A nucleotides in the DNA architecture. The GRS as a 3′ flap remained identical, and the decrease of the

fluorescence upon the addition of the same amount of FEN1 was recorded (Fig. 2a). It was found that the more T nucleotides were inserted, the fewer signal changes occurred, and the highest decrease in the fluorescence was obtained when the C34 domain was directly linked to the dumbbell substrate. The results indicated that the formation of AgNCs on the 5' flap of the DNA had a negligible influence on the recognition and cleavage of FEN1 towards the flapped DNA structure, which is in accordance with the results obtained in native-PAGE. It was reported that the enhancement effect of GRS on DNA-AgNCs reached the highest ratio when they are located close to each other [34,36]; thus, the decreased change in the fluorescence upon the increase in the number of T nucleotides correlated to the decrease in the interaction between DNA-AgNCs and the GRS.

The kinetics of the reaction at different temperatures were recorded by mixing constant concentrations of the nanoprobe and FEN1, followed by continuous detection of the fluorescent intensity at 631 nm (Fig. 2b). It was found that the fluorescence decreased as the incubation time extended. When the temperature was lower than 15 °C, a less than 10% decrease in fluorescence was recorded, which correlated to the low activity of FEN1. The highest reaction rate was found at 37 °C, in which the decrease in the fluorescence reached a plateau after 20 min of incubation. This phenomenon is reasonable because FEN1 is a nuclease mainly expressed in the cell nucleus, and 37 °C is the body temperature of humans. Extremely slow kinetics were recorded when the temperature was greater than 50 °C, which may be due to both the deactivation of FEN1 and the heating-derived conformational change in the nanoprobe. According to the calculation based on the mfold web server [55], the melting temperature (Tm) of the dumbbell DNA nanostructure is 49.5 °C. Therefore, it was assumed that when the reaction temperature was greater than 49.5 °C, the dumbbell structure of the nanoprobe would be destroyed; thus, the DNA-AgNCs and the GRS would be separated from each other, and the cleavage site of FEN1 would no longer exist. Experimental data (Figure S3) confirmed that the fluorescence of the nanoprobe significantly decreased when the temperature was greater than 50 °C, which reinforced our assumptions. Based on the results above, the optimized reaction temperature was 37 °C, and the optimized incubation time was 30 min.

3.4. Detection of FEN1

Fig. 3a shows the change in the fluorescence of this nanoprobe upon the titration of different amounts of FEN1. Decreased fluorescence was recorded along with increased amounts of FEN1, which was the result of the FEN1-induced cleavage of DNA-AgNCs. The change in fluorescence was plotted against the concentration of FEN1 (Fig. 3b), and a linear relationship from 20 to 1000 pM was obtained, yielding a limit of detection (LOD) of 10 pM and a limit of quantification (LOQ) of 33.3 pM, according to the rules of 3σ/slope and 10σ/slope, respectively. A comparison between this method and the recently published FEN1 assays is listed in Table 1. A comparable sensitivity was obtained [22,23]; however, the present nanoprobe avoided the use of organic dyes and complicated nanoscale assembly. Therefore, the present assay has higher reliability and is easier to use, which reduces the cost without sacrificing the sensitivity.

The selectivity of the nanoprobe was challenged by a wide range of interferents, including nucleases and biomolecules. T4 DNA ligase and T3 DNA ligase can catalyze the ligation of DNA gaps. Exo III can digest dsDNA from the blunt end and 5′-overhangs. The phi29 DNA polymerase and Bst DNA polymerase can extend the DNA strands with specific ends. These nucleases can change the structure of DNA molecules, thus potentially affecting the structure of the nanoprobe. Bovine serum albumin (BSA) and histone are highly concentrated proteins in buffers and cell extracts, and human serum albumin (HSA) may exist in human tissue samples. As shown in Fig. 4a, none of these interferents caused a significant decrease in the fluorescence of the nanoprobe, which indicated the selectivity of this method.

To test the specificity of the nanoprobe in targeting FEN1 in real samples, recovery tests were conducted by analyzing FEN1 in nuclear extracts from HeLa cells and clinical glioma samples. The persistent upregulation of FEN1 has been found in HeLa cervical cancer cells [56], and the overexpression of FEN1 is associated with glioma risk [57]. Therefore, the detection of FEN1 in these two samples is critical for cancer treatment. Analyzed by this method, 361.5 pM and 442.8 pM FEN1 were detected in HeLa cell and glioma extracts, respectively (Table 2). To demonstrate the accuracy of our results, we spiked the samples with exogenous FEN1, conducted the quantification, and calculated the recovery ratio (detailed in the footnote of Table 2). The recovery of this method ranged from 98.0% to 106.2%, which met the requirement for analytical methods [58–60]. The RSD of the real-sample analysis was less than 3.5%, which suggested that this method is stable [61,62]. Besides, the results obtained from our method were similar to those of commercial ELISA kits (Figure S4), while ELISA requires an extra vacuum concentration step. ELISA is a multistep assay with the involvement of unstable antibodies and enzymes, while our proposed method is a one-pot reaction without the need for enzymes.

To evaluate the repeatability of this method, samples with low

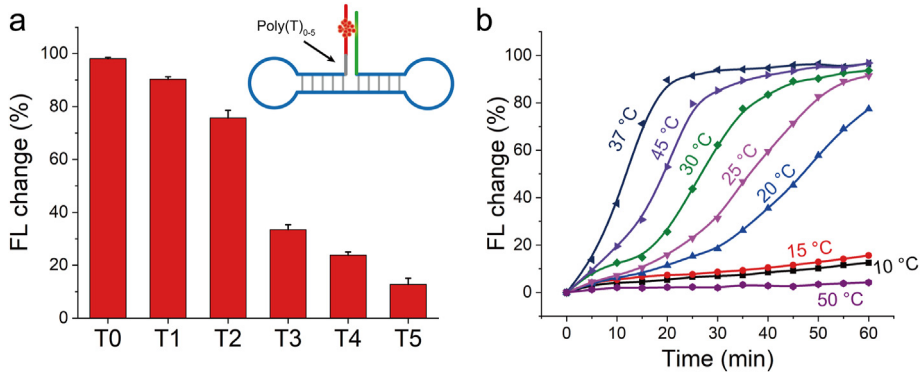

Fig. 2. Optimization of the sensing conditions in the detection of FEN1. (a) Optimization of the DNA scaffold. The inset is a sketched illustration of how the variant nanoprobes were fabricated. (b) The reaction kinetics of the optimized nanoprobe under different temperatures. The concentrations of nanoprobe and FEN1 were 20 nM in both experiments. The error bars indicate the standard deviation of three replicate determinations.

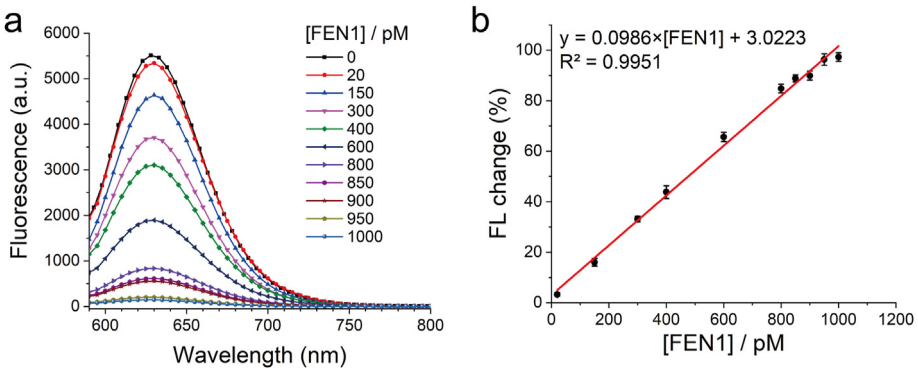

Fig. 3. The analytical performance of the nanoprobe in the detection of FEN1. (a) The change in fluorescent spectra upon the addition of various concentrations of FEN1. (b) The linear relationship between the fluorescence intensity and the concentrations of FEN1. The analysis was conducted following the methods described in the Experimental section. The error bars indicate the standard deviation of three replicate measurements.

Table 1
A comparison between this work and recent reports on the analytical methods targeting FEN1.

Detection signal	Comment	LOD	Linear range	Ref.
Fluorescent	Nanocomposite formed by graphene oxide and dye-labeled DNA.	0.38 pM	0.2–100 pM	[22]
Fluorescent	Nanoparticles assembled by DNA and gold nanoparticle. The quantification required an additional introduction of DNA-specific dye.	0.007 U	0.05–2 U	[23]
Fluorescent	Label-free and unimolecular nanoprobe that can realize one-pot detection.	10 pM	20–1000 pM	**This work**

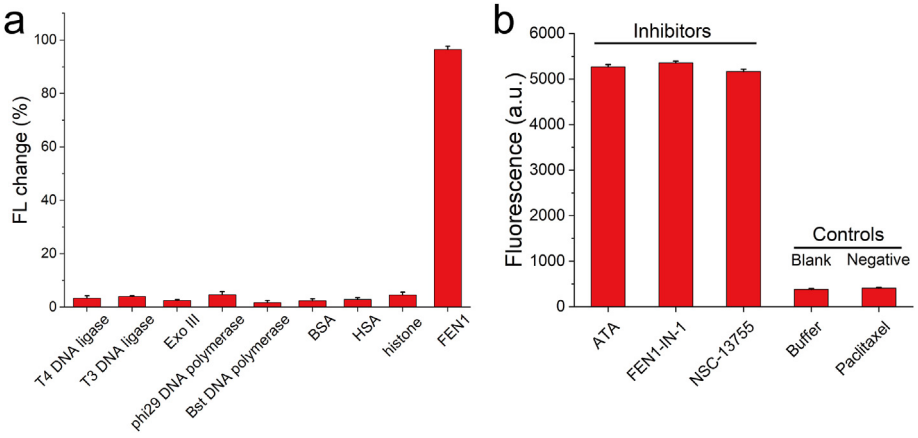

Fig. 4. (a) The selectivity of the nanoprobe towards FEN1. The concentration of FEN1 was 1 nM, while the concentrations of all the other interferents were 10 nM. (b) The evaluations of the inhibitory effects of different chemicals towards FEN1. FEN1 (1 nM) and chemicals (1 nM) were pre-incubated for 10 min, then the nanoprobe was added. The error bars represent the standard deviation of three replicate detections.

Table 2
Detection of FEN1 in nucleoproteins from cultured cells and clinical samples.

Sample	Content (pM)	Spiked (pM)	Found (pM)	Recovery (%)[a]	RSD (n = 6, %)
HeLa cells	361.5	180	552.7	106.2	3.1
		360	733.2	103.3	2.8
		540	927.5	104.8	2.4
Glioma	442.8	300	753.9	103.7	2.1
		400	860.6	104.5	3.5
		500	932.6	98.0	2.7

[a] Recovery is calculated by: Recovery = ([Found] - [Content])/[Spiked] × 100%.

(50 pM), mid (400 pM), and high (800 nM) concentrations of FEN1 in the buffer were prepared, and then the intra- and inter-day precision were investigated. As shown in Tables S2 and S3, the intra- and inter-day precision values were <3.76% and 3.79%, respectively, which indicated the precision and the repeatability of this method [63]. We also found that when storing the prepared nanoprobe at 4 °C for 20 days, the detection accuracy in analyzing low, medium, and high concentrations of FEN1 was within 15% (Figure S5). For longer storage, the nanoprobe was freeze-dried and stored at −20 °C and then dissolved prior to use. After longer storage conditions, a detection accuracy within 15% can be retained for at least 2 months (Figure S6). The above tests demonstrated the reliability, specificity, stability, and accuracy of the designed nanoprobe, which could greatly simplify the quantification of FEN1 in real samples.

3.5. Applications in the screening of FEN1 inhibitors

The dysregulation of FEN1 activity is closely related to the proliferation of cancer cells, which makes this nuclease a potent therapeutic target in pharmaceutical research [16,64,65]. The facile *in vitro* screening of FEN1 inhibitors can significantly aid the *in vivo* verification of candidate chemicals, thus it is an important task to develop robust assays for the evaluation of potential FEN1 inhibitors in cell-free systems [66–69]. We utilized a customized nanoprobe for the recognition and quantification of FEN1. Therefore, if a chemical can inhibit the activity of FEN1, it will consequently influence the fluorescence of the nanoprobe. To test this, selected chemicals were incubated with FEN1 for 20 min, followed by the addition of the same amount of nanoprobe and the measurement fluorescence (Fig. 4). Three known FEN1 inhibitors, aurintricarboxylic acid (ATA), FEN1-IN-1, and NSC-13755, hindered the cleavage of FEN1 in the nanoprobe. In comparison, a significant decrease in fluorescence was observed in the blank control (buffer) and negative control (paclitaxel). Paclitaxel is an anticancer natural product that stabilizes the polymerization of tubulin; thus, it is not surprising that it cannot inhibit FEN1. The results revealed that this method can be applied in screening FEN1 inhibitors.

4. Conclusion

In this work, a nanoprobe based on fluorescence tunable DNA-AgNCs was rationally designed for the detection of FEN1. To realize the recognition of FEN1, the nanoprobe was designed to have two flaps at both the 3′ and 5′ ends of a dumbbell-shaped DNA structure. FEN1 exhibits intrinsic enzymatic activity to remove the 5′ flap of the DNA molecules; however, whether FEN1 could remove a 5' flap functionalized with nanomaterial remained unknown. Our study revealed that FEN1 can function in a DNA-AgNC-embedded DNA domain, by cleaving the flap with DNA-AgNCs. This FEN1-specific reaction separated DNA-AgNCs from the GRS, impeding the close interaction between DNA-AgNCs and the GRS, and resulting in a decrease in the fluorescence. Derived from the high performance of DNA-AgNCs in biosensing, this nanoprobe allowed sensitive detection of FEN1 with picomolar sensitivity. The specificity and robustness have also been indicated by analyzing the real sample and screening FEN1 inhibitors. Therefore, this work customized a nanoprobe composed of DNA-AgNCs for the sensing of FEN1 based on the enzymatic activity of the target, and we envision that this nanoprobe can facilitate both cancer diagnosis and drug development.

CRediT authorship contribution statement

Bingzhi Li: Visualization, Investigation, Writing - review & editing, Supervision. **Peng Zhang:** Visualization, Investigation, Writing - review & editing. **Bin Zhou:** Validation. **Siying Xie:** Data curation. **Anqi Xia:** Writing - review & editing. **Tiying Suo:** Methodology. **Shuang Feng:** Data curation, Supervision. **Xing Zhang:** Writing - review & editing, Supervision.

Declaration of competing interest

The authors declare that they have no known competing financial interests or personal relationships that could have appeared to influence the work reported in this paper.

Acknowledgments

This work was supported by grants from the Natural Science Foundation of Jiangsu Province (No. BK20200718 and BK20200728), the National Natural Science Foundation of China (No. 22007049), the Natural Science Foundation of the Jiangsu Higher Education Institutions of China (20KJB350010), and the Scientific Research Start-Up Funding for Nanjing Normal University Introduced Talents (184080H202B246). T.Y.S. acknowledges funding from the Postgraduate Research & Practice Innovation Program of Jiangsu Province (KYCX20_1261).

Appendix A. Supplementary data

Supplementary data to this article can be found online at https://doi.org/10.1016/j.aca.2020.12.069.

References

[1] B. Shen, L.F. Wang, X. Zhi, Y. Qian, Construction of a red emission BODIPY-based probe for tracing lysosomal viscosity changes in culture cells, Sensor. Actuator. B Chem. 304 (2020) 127271, https://doi.org/10.1016/j.snb.2019.127271.
[2] J. Wang, Q. Lu, C. Weng, X. Li, X. Yan, W. Yang, B. Li, X. Zhou, Label-free colorimetric detection of acid phosphatase and screening of its inhibitors based on biomimetic oxidase activity of MnO2 nanosheets, ACS Biomater. Sci. Eng. 6 (2020) 3132−3138, https://doi.org/10.1021/acsbiomaterials.0c00217.
[3] N. Choi, H. Dang, A. Das, M.S. Sim, I.Y. Chung, J. Choo, SERS biosensors for ultrasensitive detection of multiple biomarkers expressed in cancer cells, Biosens. Bioelectron. 164 (2020) 112326, https://doi.org/10.1016/j.bios.2020.112326.
[4] R. Han, G. Wang, Z. Xu, L. Zhang, Q. Li, Y. Han, X. Luo, Designed antifouling peptides planted in conducting polymers through controlled partial doping for electrochemical detection of biomarkers in human serum, Biosens. Bioelectron. 164 (2020) 112317, https://doi.org/10.1016/j.bios.2020.112317.
[5] B. Li, A. Xia, S. Zhang, T. Suo, Y. Ma, H. Huang, X. Zhang, Y. Chen, X. Zhou, A CRISPR-derived biosensor for the sensitive detection of transcription factors based on the target-induced inhibition of Cas12a activation, Biosens. Bioelectron. 173 (2021) 112619, https://doi.org/10.1016/j.bios.2020.112619.
[6] B. Li, T. Suo, S. Xie, A. Xia, Y. Ma, H. Huang, X. Zhang, Q. Hu, Rational design, synthesis, and applications of carbon dots@metal−organic frameworks (CD@MOF) based sensors, Trac. Trends Anal. Chem. (2020) 116163, https://doi.org/10.1016/j.trac.2020.116163.
[7] R.S. Williams, T.A. Kunkel, FEN nucleases: bind, bend, fray, cut, Cell 145 (2011) 171−172, https://doi.org/10.1016/j.cell.2011.03.039.
[8] S.E. Tsutakawa, A.H. Sarker, C. Ng, A.S. Arvai, D.S. Shin, B. Shih, S. Jiang, A.C. Thwin, M. Tsai, A. Willcox, M.Z. Her, K.S. Trego, A.G. Raetz, D. Rosenberg, A. Bacolla, M. Hammel, J.D. Griffith, P.K. Cooper, J.A. Tainer, Human XPG nuclease structure, assembly, and activities with insights for neurodegeneration and cancer from pathogenic mutations, Proc. Natl. Acad. Sci. Unit. States Am. 117 (2020) 14127−14138, https://doi.org/10.1073/pnas.1921311117.
[9] N. Patel, J.C. Exell, E. Jardine, B. Ombler, L.D. Finger, B. Ciani, J.A. Grasby, Proline scanning mutagenesis reveals a role for the flap endonuclease-1 helical cap in substrate unpairing, J. Biol. Chem. 288 (2013) 34239−34248, https://doi.org/10.1074/jbc.M113.509489.
[10] H. Debrauwere, S. Loeillet, W. Lin, J. Lopes, A. Nicolas, Links between replication and recombination in Saccharomyces cerevisiae: a hypersensitive requirement for homologous recombination in the absence of Rad27 activity, Proc. Natl. Acad. Sci. Unit. States Am. 98 (2001) 8263−8269, https://doi.org/10.1073/pnas.121075598.
[11] S.E. Tsutakawa, S. Classen, B.R. Chapados, A.S. Arvai, L.D. Finger, G. Guenther, C.G. Tomlinson, P. Thompson, A.H. Sarker, B. Shen, P.K. Cooper, J.A. Grasby,

J.A. Tainer, Human flap endonuclease structures, DNA double-base flipping, and a unified understanding of the FEN1 superfamily, Cell 145 (2011) 198–211, https://doi.org/10.1016/j.cell.2011.03.004.
[12] S. Ba, H. Zhang, J.Y. Lee, H. Wu, R. Ye, D. Huang, T. Li, Investigation of human flap structure-specific endonuclease 1 (FEN1) activity on primer-template models and exploration of a substrate-based FEN1 inhibitor, Bioorg. Med. Chem. 24 (2016) 1988–1992, https://doi.org/10.1016/j.bmc.2016.03.025.
[13] L.D. Finger, M.S. Blanchard, C.A. Theimer, B. Sengerová, P. Singh, V. Chavez, F. Liu, J.A. Grasby, B. Shen, The 3′-flap pocket of human flap endonuclease 1 is critical for substrate binding and catalysis, J. Biol. Chem. 284 (2009) 22184–22194, https://doi.org/10.1074/jbc.M109.015065.
[14] X. Xin, T. Wen, L. Gong, M. Deng, K. Hou, L. Xu, S. Shi, X. Qu, Y. Liu, X. Che, Y. Teng, Inhibition of FEN1 increases arsenic trioxide-induced ROS accumulation and cell death: novel therapeutic potential for triple negative breast cancer, Frontiers in Oncology 10 (2020), https://doi.org/10.3389/fonc.2020.00425.
[15] K.D. Flach, M. Periyasamy, A. Jadhav, D. Dorjsuren, J.C. Siefert, T.E. Hickey, M. Opdam, H. Patel, S. Canisius, D.M. Wilson, M. Donaldson Collier, S. Prekovic, M. Nieuwland, R.J.C. Kluin, A.V. Zakharov, J. Wesseling, L.F.A. Wessels, S.C. Linn, W.D. Tilley, A. Simeonov, S. Ali, W. Zwart, Endonuclease FEN1 coregulates ERα activity and provides a novel drug interface in tamoxifen-resistant breast cancer, Canc. Res. 80 (2020) 1914–1926, https://doi.org/10.1158/0008-5472.CAN-19-2207.
[16] L. He, Y. Zhang, H. Sun, F. Jiang, H. Yang, H. Wu, T. Zhou, S. Hu, C.S. Kathera, X. Wang, H. Chen, H. Li, B. Shen, Y. Zhu, Z. Guo, Targeting DNA flap endonuclease 1 to impede breast cancer progression, EBioMedicine 14 (2016) 32–43, https://doi.org/10.1016/j.ebiom.2016.11.012.
[17] J.S. Lam, D.B. Seligson, H. Yu, A.I. Li, M. Eeva, A.J. Pantuck, G. Zeng, S. Horvath, A.S. Belldegrun, Flap endonuclease 1 is overexpressed in prostate cancer and is associated with a high Gleason score, BJU Int. 98 (2006) 445–451, https://doi.org/10.1111/j.1464-410X.2006.06224.x.
[18] T.M.A. Abdel-Fatah, R. Russell, N. Albarakati, D.J. Maloney, D. Dorjsuren, O.M. Rueda, P. Moseley, V. Mohan, H. Sun, R. Abbotts, A. Mukherjee, D. Agarwal, J.L. Illuzzi, A. Jadhav, A. Simeonov, G. Ball, S. Chan, C. Caldas, I.O. Ellis, D.M. Wilson, S. Madhusudan, Genomic and protein expression analysis reveals flap endonuclease 1 (FEN1) as a key biomarker in breast and ovarian cancer, Molecular Oncology 8 (2014) 1326–1338, https://doi.org/10.1016/j.molonc.2014.04.009.
[19] L.N. Tumey, D. Bom, B. Huck, E. Gleason, J. Wang, D. Silver, K. Brunden, S. Boozer, S. Rundlett, B. Sherf, S. Murphy, T. Dent, C. Leventhal, A. Bailey, J. Harrington, Y.L. Bennani, The identification and optimization of a N-hydroxy urea series of flap endonuclease 1 inhibitors, Bioorg. Med. Chem. Lett 15 (2005) 277–281, https://doi.org/10.1016/j.bmcl.2004.10.086.
[20] L. He, Y. Zhang, H. Sun, F. Jiang, H. Yang, H. Wu, T. Zhou, S. Hu, C.S. Kathera, X. Wang, H. Chen, H. Li, B. Shen, Y. Zhu, Z. Guo, Targeting DNA flap endonuclease 1 to impede breast cancer progression, EBioMedicine 14 (2016) 32–43, https://doi.org/10.1016/j.ebiom.2016.11.012.
[21] L. Ma, X. Cao, H. Wang, K. Lu, Y. Wang, C. Tu, Y. Dai, Y. Meng, Y. Li, P. Yu, S. Man, A. Diao, Discovery of myricetin as a potent inhibitor of human flap endonuclease 1, which potentially can Be used as sensitizing agent against HT-29 human colon cancer cells, J. Agric. Food Chem. 67 (2019) 1656–1665, https://doi.org/10.1021/acs.jafc.8b05447.
[22] H. Zhang, S. Ba, D. Mahajan, J.Y. Lee, R. Ye, F. Shao, L. Lu, T. Li, Versatile types of DNA-based nanobiosensors for specific detection of cancer biomarker FEN1 in living cells and cell-free systems, Nano Lett. 18 (2018) 7383–7388, https://doi.org/10.1021/acs.nanolett.8b03724.
[23] C. Wang, D. Zhang, Y. Tang, W. Wei, Y. Liu, S. Liu, Label-free imaging of flap endonuclease 1 in living cells by assembling original and multifunctional nanoprobe, ACS Applied Bio Materials 3 (2020) 4573–4580, https://doi.org/10.1021/acsabm.0c00494.
[24] B. Li, Y. Chen, J. Wang, Q. Lu, W. Zhu, J. Luo, J. Hong, X. Zhou, Detecting transcription factors with allosteric DNA-Silver nanocluster switches, Anal. Chim. Acta 1048 (2019) 168–177, https://doi.org/10.1016/j.aca.2018.10.023.
[25] Y. Du, B. Li, E. Wang, "Fitting" makes "sensing" simple: label-free detection strategies based on nucleic acid aptamers, Accounts Chem. Res. 46 (2012) 203–213, https://doi.org/10.1021/ar300011g.
[26] C. Leung, K. Wu, G. Li, C. Wu, C. Ko, D. Ma, Application of label-free techniques in microfluidic for biomolecules detection and circulating tumor cells analysis, Trac. Trends Anal. Chem. 117 (2019) 78–83, https://doi.org/10.1016/j.trac.2019.06.003.
[27] G. Dutta, J. Rainbow, U. Zupancic, S. Papamatthaiou, P. Estrela, D. Moschou, Microfluidic devices for label-free DNA detection, Chemosensors 6 (2018) 43, https://doi.org/10.3390/chemosensors6040043.
[28] D. Ma, H. He, K. Leung, H. Zhong, D.S. Chan, C. Leung, Label-free luminescent oligonucleotide-based probes, Chem. Soc. Rev. 42 (2013) 3427, https://doi.org/10.1039/c2cs35472a.
[29] T. Suo, M. Sohail, Y. Ma, B. Li, Y. Chen, X. Zhang, X. Zhou, A versatile turn-on fluorometric biosensing profile based on split aptamers-involved assembly of nanocluster beacon sandwich, Sensor. Actuator. B Chem. 324 (2020) 128586, https://doi.org/10.1016/j.snb.2020.128586.
[30] G. Liu, J. Li, D. Feng, J. Zhu, W. Wang, Silver nanoclusters beacon as stimuli-responsive versatile platform for multiplex DNAs detection and aptamer–substrate complexes sensing, Anal. Chem. 89 (2017) 1002–1008, https://doi.org/10.1021/acs.analchem.6b04362.
[31] Y. Guo, F. Shen, Y. Cheng, Y. Xie, H. Yu, W. Yao, H. Li, H. Qian, R. Pei, The light-up fluorescence of AgNCs in a "DNA bulb.", Nanoscale 10 (2018) 11517–11523, https://doi.org/10.1039/C8NR02575D.
[32] Z. Luo, K. Zheng, J. Xie, Engineering ultrasmall water-soluble gold and silver nanoclusters for biomedical applications, Chem. Commun. 50 (2014) 5143–5155, https://doi.org/10.1039/C3CC47512C.
[33] Y. Tao, M. Li, J. Ren, X. Qu, Metal nanoclusters: novel probes for diagnostic and therapeutic applications, Chem. Soc. Rev. 44 (2015) 8636–8663, https://doi.org/10.1039/C5CS00607D.
[34] Y. Chen, M.L. Phipps, J.H. Werner, S. Chakraborty, J.S. Martinez, DNA templated metal nanoclusters: from emergent properties to unique applications, Accounts Chem. Res. 51 (2018) 2756–2763, https://doi.org/10.1021/acs.accounts.8b00366.
[35] J.M. Obliosca, M.C. Babin, C. Liu, Y. Liu, Y. Chen, R.A. Batson, M. Ganguly, J.T. Petty, H. Yeh, A complementary palette of NanoCluster beacons, ACS Nano 8 (2014) 10150–10160, https://doi.org/10.1021/nn505338e.
[36] Y. Chen, H.T. Vu, Y. Liu, Y. Chen, T.D. Nguyen, Y. Kuo, S. Hong, Y. Chen, S. Carnahan, J.T. Petty, H. Yeh, Improving NanoCluster Beacon performance by blocking the unlabeled NC probes, Chem. Commun. 55 (2019) 462–465, https://doi.org/10.1039/C8CC08291J.
[37] T. Suo, M. Sohail, S. Xie, B. Li, Y. Chen, L. Zhang, X. Zhang, DNA nanotechnology: a recent advancement in the monitoring of microcystin-LR, J. Hazard Mater. 403 (2021) 123418, https://doi.org/10.1016/j.jhazmat.2020.123418.
[38] S.Y. New, S.T. Lee, X.D. Su, DNA-templated silver nanoclusters: structural correlation and fluorescence modulation, Nanoscale 8 (2016) 17729–17746, https://doi.org/10.1039/C6NR05872H.
[39] H. Yeh, J. Sharma, J.J. Han, J.S. Martinez, J.H. Werner, A DNA–Silver nanocluster probe that fluoresces upon hybridization, Nano Lett. 10 (2010) 3106–3110, https://doi.org/10.1021/nl101773c.
[40] S.H. Yau, N. Abeyasinghe, M. Orr, L. Upton, O. Varnavski, J.H. Werner, H. Yeh, J. Sharma, A.P. Shreve, J.S. Martinez, T. Goodson III, Bright two-photon emission and ultra-fast relaxation dynamics in a DNA-templated nanocluster investigated by ultra-fast spectroscopy, Nanoscale 4 (2012) 4247, https://doi.org/10.1039/c2nr30628j.
[41] S. Zhang, K. Wang, K. Li, W. Shi, W. Jia, X. Chen, T. Sun, D. Han, A DNA-stabilized silver nanoclusters/graphene oxide-based platform for the sensitive detection of DNA through hybridization chain reaction, Biosens. Bioelectron. 91 (2017) 374–379, https://doi.org/10.1016/j.bios.2016.12.060.
[42] L. Gong, H. Kuai, S. Ren, X.H. Zhao, S.Y. Huan, X.B. Zhang, W. Tan, Ag nanocluster-based label-free catalytic and molecular beacons for amplified biosensing, Chem. Commun. 51 (2015) 12095–12098, https://doi.org/10.1039/c5cc04442a.
[43] B. Li, L. Xu, Y. Chen, W. Zhu, X. Shen, C. Zhu, J. Luo, X. Li, J. Hong, X. Zhou, Sensitive and label-free fluorescent detection of transcription factors based on DNA-Ag nanoclusters molecular beacons and exonuclease III-assisted signal amplification, Anal. Chem. 89 (2017) 7316–7323, https://doi.org/10.1021/acs.analchem.7b00055.
[44] B. Li, Y. Chen, J. Wang, Q. Lu, W. Zhu, L. Xu, X. Shen, J. Luo, C. Zhu, X. Li, J. Hong, X. Zhou, DNA-silver nanoclusters/polypyrrole nanoparticles: a label-free and enzyme-free platform for multiplexed transcription factors detection, Sensor. Actuator. B Chem. 274 (2018) 481–490, https://doi.org/10.1016/j.snb.2018.07.152.
[45] L. Ge, X. Sun, Q. Hong, F. Li, Ratiometric NanoCluster beacon: a label-free and sensitive fluorescent DNA detection platform, ACS Appl. Mater. Interfaces 9 (2017) 13102–13110, https://doi.org/10.1021/acsami.7b03198.
[46] M. Peng, N. Na, J. Ouyang, A fluorescence light-up silver nanocluster beacon modulated by metal ions and its application in telomerase-activity detection, Chem. Eur J. 25 (2019) 3598–3605, https://doi.org/10.1002/chem.201805308.
[47] R. Jin, Atomically precise metal nanoclusters: stable sizes and optical properties, Nanoscale 7 (2015) 1549–1565, https://doi.org/10.1039/C4NR05794E.
[48] J.M. Obliosca, C. Liu, H.C. Yeh, Fluorescent silver nanoclusters as DNA probes, Nanoscale 5 (2013) 8443–8461, https://doi.org/10.1039/c3nr01601c.
[49] J. Wu, N. Li, Y. Yao, D. Tang, D. Yang, J. Ong Achwa Machuki, J. Li, Y. Yu, F. Gao, DNA-stabilized silver nanoclusters for label-free fluorescence imaging of cell surface glycans and fluorescence guided photothermal therapy, Anal. Chem. 90 (2018) 14368–14375, https://doi.org/10.1021/acs.analchem.8b03837.
[50] I.L. Volkov, A. Smirnova, A.A. Makarova, Z.V. Reveguk, R.R. Ramazanov, D.Y. Usachov, V.K. Adamchuk, A.I. Kononov, DNA with ionic, atomic, and clustered silver: an XPS study, J. Phys. Chem. B 121 (2017) 2400–2406, https://doi.org/10.1021/acs.jpcb.6b11218.
[51] D. Feng, G. Liu, W. Wang, A novel biosensor for copper(ii) ions based on turn-on resonance light scattering of ssDNA templated silver nanoclusters, J. Mater. Chem. B. 3 (2015) 2083–2088, https://doi.org/10.1039/C4TB01940G.
[52] Y. Teng, X. Jia, S. Zhang, J. Zhu, E. Wang, A nanocluster beacon based on the template transformation of DNA-templated silver nanoclusters, Chem. Commun. 52 (2016) 1721–1724, https://doi.org/10.1039/C5CC09138A.
[53] J. Zhang, C. Li, X. Zhi, G.A. Ramón, Y. Liu, C. Zhang, F. Pan, D. Cui, Hairpin DNA-templated silver nanoclusters as novel beacons in strand displacement amplification for MicroRNA detection, Anal. Chem. 88 (2015) 1294–1302, https://doi.org/10.1021/acs.analchem.5b03729.
[54] H. Que, D. Zhang, B. Guo, T. Wang, H. Wu, D. Han, Y. Yan, Label-free and ultrasensitive electrochemical biosensor for the detection of EBV-related DNA based on AgDNCs@DNA/AgNCs nanocomposites and lambda exonuclease-assisted target recycling, Biosens. Bioelectron. 143 (2019) 111610, https://doi.org/10.1016/j.bios.2019.111610.
[55] M. Zuker, Mfold web server for nucleic acid folding and hybridization

prediction, Nucleic Acids Res. 31 (2003) 3406–3415, https://doi.org/10.1093/nar/gkg595.
[56] J.L. Li, J.P. Wang, H. Chang, S.M. Deng, J.H. Du, X.X. Wang, H.J. Hu, D.Y. Li, X.B. Xu, W.Q. Guo, Y.H. Song, Z. Guo, M.X. Sun, Y.W. Wu, S.B. Liu, FEN1 inhibitor increases sensitivity of radiotherapy in cervical cancer cells, Cancer Medicine 8 (2019) 7774–7780, https://doi.org/10.1002/cam4.2615.
[57] Y. Chen, X. Zhang, X. Qiu, J. Li, Q. Yuan, T. Jiang, M. Yang, Functional FEN1 genetic variants and haplotypes are associated with glioma risk, J. Neuro Oncol. 111 (2013) 145–151, https://doi.org/10.1007/s11060-012-1007-0.
[58] M. Thompson, S.L.R. Ellison, A. Fajgelj, P. Willetts, R. Wood, Harmonized guidelines for the use of recovery information in analytical measurement, Pure Appl. Chem. 71 (1999) 337–348, https://doi.org/10.1351/pac199971020337.
[59] J. Duffus, Glossary for chemists of terms used in toxicology (IUPAC Recommendations 1993), Pure Appl. Chem. 65 (1993) 2003–2122, https://doi.org/10.1351/pac199365092003.
[60] U. S. F. A. Administration: Guidelines for the Validation of Chemical Methods in Food, Feed, Cosmetics, and Veterinary Products, 2019.
[61] L.A. Currie, G. Svehla, Nomenclature for the presentation of results of chemical analysis (IUPAC Recommendations 1994), Pure Appl. Chem. 66 (1994) 595–608, https://doi.org/10.1351/pac199466030595.
[62] U. S. F. A. Administration: Bioanalytical Method Validation Guidance for Industry, 2018.
[63] W. Zhou, F. Xu, D. Li, Y. Chen, Improved detection of HER2 by a quasi-targeted proteomics approach using aptamer–peptide probe and liquid chromatography–tandem mass spectrometry, Clin. Chem. 64 (2018) 526–535, https://doi.org/10.1373/clinchem.2017.274266.
[64] J.L. Li, J.P. Wang, H. Chang, S.M. Deng, J.H. Du, X.X. Wang, H.J. Hu, D.Y. Li, X.B. Xu, W.Q. Guo, Y.H. Song, Z. Guo, M.X. Sun, Y.W. Wu, S.B. Liu, FEN1 inhibitor increases sensitivity of radiotherapy in cervical cancer cells, Cancer Medicine 8 (2019) 7774–7780, https://doi.org/10.1002/cam4.2615.
[65] L. He, H. Yang, S. Zhou, H. Zhu, H. Mao, Z. Ma, T. Wu, A.K. Kumar, C. Kathera, A. Janardhan, F. Pan, Z. Hu, Y. Yang, L. Luo, Z. Guo, Synergistic antitumor effect of combined paclitaxel with FEN1 inhibitor in cervical cancer cells, DNA Repair 63 (2018) 1–9, https://doi.org/10.1016/j.dnarep.2018.01.003.
[66] R.U. Agu, M.I. Ugwoke, In vitro andin vivo testing methods for respiratory drug delivery, Expet Opin. Drug Deliv. 8 (2010) 57–69, https://doi.org/10.1517/17425247.2011.543896.
[67] J. Nie, Q. Gao, J. Fu, Y. He, Grafting of 3D bioprinting to in vitro drug screening: a Review, Adv. Healthc. Mater. 9 (2020) 1901773, https://doi.org/10.1002/adhm.201901773.
[68] P. Vacchina, M.A. Morales, In vitro screening test using leishmania promastigotes stably expressing mCherry protein, Antimicrob. Agents Chemother. 58 (2014) 1825–1828, https://doi.org/10.1128/AAC.02224-13.
[69] R.U. Agu, M.I. Ugwoke, In vitro andin vivo testing methods for respiratory drug delivery, Expet Opin. Drug Deliv. 8 (2010) 57–69, https://doi.org/10.1517/17425247.2011.543896.